Effectiveness of active flow control for turbulent skin friction drag reduction

Yongmann M Chung* **and Tariq Talha**

School of Engineering and Centre for Scientific Computing,

University of Warwick, Coventry, CV4 7AL, U.K.

[Final Manuscript]

January 11, 2011

Abstract

The effectiveness of the opposition control method proposed by Choi *et al.* [H. Choi, P. Moin, and J. Kim, *J. Fluid Mech.* **262**, 75–110 (1994)] has been studied using direct numerical simulations. In this study, the effects of the amplitude and the phase of wall blowing and suction control input were considered separately. It is found that the amplitude of wall blowing and suction as well as the detection plane location played an important role in active control for skin friction drag reduction. By changing the amplitude, a substantial drag reduction was achieved for all detection plane locations considered, and the efficiency of the opposition control was also improved. When the control was effective, the drag reduction was proportional to the wall blowing and suction strength. There existed a maximum wall blowing and suction strength, beyond which the opposition control became less effective or even unstable. Turbulence characteristics affected by various wall blowing and suction parameters were analysed to understand

*Corresponding author: Y.M.Chung@warwick.ac.uk

the underlying mechanisms for drag reduction. The wall normal velocity and vorticity fluctuations showed a strong correlation with drag reduction.

Keywords: Flow control; active control; opposition control; skin friction; drag reduction; blowing and suction; streamwise vortices

1 Introduction

Effective and reliable flow control to reduce turbulent skin friction drag is of paramount importance in many engineering applications, including aerospace engineering, where the skin friction component is approximately one quarter of the total aircraft drag in flight condition [1]. Various control strategies have been developed for turbulent drag reduction [2, 3], with many of them focusing on the manipulation of the near-wall turbulence structures, such as streamwise vortices, which are responsible for most of turbulent kinetic energy production [4, 5]. Among other control methods, active control using wall blowing and suction [6] has attracted significant interest in relation to potential, micro-electro-mechanical systems (MEMS) based boundary layer control [7–10]. Choi *et al.* [6] proposed the opposition control, in which wall blowing and suction were determined by the wall-normal velocity in the buffer layer. A schematic diagram of the opposition control is shown in Figure 1. They reported that this control method weakened effectively the streamwise vortices and an approximately $20 - 25\%$ of drag reduction was observed. Their study demonstrated that turbulent drag reductions could be achieved by simple closed loop control using wall blowing and suction.

The opposition control method has proved to be very useful for developing more practical control strategies which utilised only wall information [11–13]. For example, in the suboptimal control, Lee *et al.* [12] analysed the opposition controlled flow field with $y_d^+ = 10$ to find that wall distributions of dp/dz and dw/dy fluctuations could be used to determine the control input, and in the wall deformation flow control [14, 15] the velocity induced by wall motion was set equal to the velocity at the detection plane of the opposition control (with $y_d^+ = 10$). To provide more realistic wall actuation, dimples were used as an actuator for opposition control numerically [16] and experimentally [17]. Carlson and Lumley [16] used a Gaussian bump to prevent a downwash of high-momentum fluids towards the wall during the sweep events. Kim *et al.* [17] used a dimple oscillating at near the bursting frequency. The applicability of the opposition control method was later extended to higher Reynolds number flows; a substantial drag reduction was still achieved at $Re_\tau = 640$ [18] and $Re_\tau = 720$ [19]. Pamies *et al.* [20] reported a 17.9% drag reduction for $Re_\tau = 960$. Recently, the opposition control has been applied in experiment using

both the off-line [17, 21] and real-time [10, 22] control.

In the opposition control, the wall blowing and suction were in opposition to the wall-normal velocity at the detection plane (y_d) [6]:

$$v(x, 0, z; t) = -v(x, y_d, z; t), \tag{1}$$

where, x, y and z are the streamwise, wall normal, and spanwise coordinates, respectively, and t the time. In this study, u, v and w are velocity component in the x, y and z directions, respectively. The effect of the detection plane location on the drag reduction of the opposition control method was first investigated by Choi *et al.* [6]. They focused on the optimal detection plane location for drag reduction, and suggested that the detection plane at $y_d^+ = 10$ was optimal at a Re number of $Re_\tau = 180$. Later, Hammond *et al.* [23], and Chung and Sung [24] reported that a detection plane at $y_d^+ = 15$ gave a slightly better drag reduction. The importance of the optimal detection plane location ($y_{d,op}^+$) for the turbulent skin-friction drag reduction has been well studied. However, the effect of the strength of the wall blowing and suction on the effectiveness of the opposition control is not fully understood. Only limited studies were carried out in this regard [18, 24]. An amplitude of 20% was tested with the detection plane at $y_d^+ = 10$ by Iwamoto *et al.* [18]. Chung and Sung [24] found that a significant amount of drag reduction was still obtained when the amplitude of the wall blowing and suction was halved for the detection plane at $y_d^+ = 20$. This suggests that the efficiency of the opposition control can be improved by using less power input. Since the power input for the opposition control is proportional to the cube of the wall blowing and suction velocity, understanding the relationship between the amplitude of opposition control and drag reduction is important for an efficient flow control strategy.

The main objective of this study was to explore the effectiveness of the opposition control with a view to enhancing the operating range of the opposition control using smaller amplitudes. The separate effects of the amplitude and the detection plane location of opposition control were investigated. To this end, direct numerical simulations (DNS) were performed with various wall blowing and suction amplitudes at nine detection plane

locations. Another objective of the present study was to understand the characteristics of the optimally controlled flow to find common features of drag reduction. Controlled flow fields were analysed to examine the relationship between the various flow properties and the amount of drag reduction. This knowledge can be used to suggest how turbulence needs to be modified for better drag reduction, and is therefore useful in developing a future optimal control strategy.

2 Numerical methods

Results presented in this paper have been computed using a second-order finite volume DNS code [25–27]. The convective terms were modelled using a third-order Runge-Kutta method, and the diffusive terms using the Crank-Nicolson method. A fractional step method was used for time advancement. The flow was assumed to be periodic in the streamwise and spanwise directions. All flow variables were nondimensionalized by the bulk-mean velocity U_m and the channel half-depth h. The Reynolds number was $Re(\equiv U_m h/\nu) = 2800$, where ν is the kinematic viscosity of the fluid. The Re number based on the friction velocity (u_τ) of the uncontrolled case was $Re = u_{\tau_0} h/\nu = 180$, here the subscript 0 indicates values for the no-control case. The computational domain had dimensions $2\pi \times 2 \times \pi/2$ in x, y and z directions, respectively. A $64 \times 129 \times 64$ grid was used in the study, and the corresponding grid spacings were $\Delta x^+ = 17.7$, $\Delta y^+_{min} = 0.2$, $\Delta y^+_{max} = 7.0$ and $\Delta z^+ = 4.7$. The time step used was kept smaller than $\Delta t^+ (= \Delta t u_\tau^2/\nu) = 0.4$ [28] during the simulation, and the total time for sampling was $600h/U_m$. Several simulations were repeated with a larger computational domain to ascertain that the results were not influenced by the size of the computational domain. For this, a computational domain of $14 \times 2 \times 3.5$ was used with a $128 \times 129 \times 128$ grid. Only a small difference was observed between the two domain sizes for both no-control and control cases, indicating that the domain size used in this study was adequate.

Table 1: Numerical parameters used in direct numerical simulations. y_d^+ is the detection plane location in wall units. Two friction velocities are used: the no-control case u_{τ_0} value and the local u_τ value. $v'(y_d^+)$ and $v'^+(y_d^+)$ is rms wall normal velocity fluctuation of the no-control case at y_d^+ in global and wall units, respectively.

Case	y_d^+ (nominal value)	y_d^+ (based on u_{τ_0})	y_d^+ (based on u_τ)	$v'(y_d^+)$	$v'^+(y_d^+)$
Case 1	5	4.82	4.58	0.0031	0.047
Case 2	10	9.89	8.83	0.0102	0.155
Case 3	13	12.98	11.26	0.0148	0.235
Case 4	15	15.43	13.32	0.0194	0.395
Case 5	17	16.79	14.68	0.0226	0.344
Case 6	20	19.81	18.12	0.0303	0.461
Case 7	23	23.27	25.08	0.0450	0.686
Case 8	25	25.17	30.47	0.0572	0.872
Case 9	30	29.38	40.41	0.0708	1.079

3 Results and Discussion

In this study, the flow rate in the streamwise direction was kept constant during the simulation, allowing the mean pressure gradient to change. Drag reduction was measured by a change in the wall shear stress (τ_w):

$$\mathrm{DR} = 1 - \frac{\tau_w}{\tau_{w0}} = 1 - \left(\frac{u_\tau}{u_{\tau 0}}\right)^2, \tag{2}$$

where, DR represents a drag reduction. In opposition control, the magnitude of blowing and suction was the opposite to the wall-normal velocity at a detection plane located at a small distance (y_d) from the wall (see Figure 1). In this study, we introduced an amplitude parameter, A, to describe the strength of wall blowing and suction:

$$v(x, 0, z; t) = -Av(x, y_d, z; t). \tag{3}$$

It is worth noting that $A = 1$ was used in the previous studies [6, 19, 23], and that the effect of blowing and suction amplitude was not examined.

3.1 Detection plane location

First, the effect of the detection plane location on drag reduction of the opposition control method is re-examined. As mentioned earlier, the optimal detection plane location was investigated first by Choi *et al.* [6] and later by several researchers including Hammond *et al.* [23], Chang *et al.* [19] and Chung and Sung [24]. The purpose of this study was not to identify the optimal detection plane location, but to examine the relationship between velocity data from different detection plane locations. For this, the amplitude parameter was set to be $A = 1$, and nine different detection plane locations were considered in a range of $5 \leq y_d^+ \leq 30$. In the opposition control, the vertical velocity information was required on the detection plane. No interpolation was applied in this study to obtain the velocity at a detection plane. Instead, the detection plane location was chosen among vertical grid points. Please note that the detection plane for $y_d^+ = 15$ was not located exactly at $y_d^+ = 15$ but at the nearest grid point around the nominal value, which was, in this case, at $y_d^+ = 15.4$ based on u_{τ_0}, and $y_d^+ = 13.5$ based on the local u_τ value. Simulation parameters are summarised in Table 1, and the nominal values in the table are referred to as the detection plane locations in the analysis hereafter.

All simulations were started with the fully developed velocity field of the no-control case. The time history of the friction Reynolds number, Re_τ, is shown in Figure 2 for various detection plane locations. It is shown from the figure that the overall success of opposition control is sensitive to the location of a detection plane. For $y_d^+ \leq 20$, drag reduction is achieved with varying degrees of success while Re_τ increases significantly for $y_d^+ > 20$. The optimal opposition control is found at $y_d^+ \approx 15$, consistent with Hammond *et al.* (1998) and Chung and Sung [24]. With the carefully chosen detection plane at $y_d^+ = 15$, a drag reduction of 25% is observed from DNS. It is clearly seen that the detection planes at $y_d^+ = 25$ and 30 result in a large drag increase [6, 23, 24]. It is worth noting that the optimal detection locations were found to move closer to the wall as Re increased [19]. The detection plane location decreased from $y_{d,op}^+ = 15$ for $Re_\tau = 180$ to $y_{d,op}^+ = 12.5$ for $Re_\tau = 720$. Pamies *et al.* [20] used the detection plane location at $y_{d,op}^+ = 11.5$ for $Re_\tau = 960$. It should be noted that our findings in this study are based on the DNS study of $Re_\tau = 180$.

The time-averaged drag reduction is calculated using Equation 2, and is shown in Figure 3. Negative values of DR indicate a drag increase. The amount of drag reduction increases almost linearly as the detection plane moves away from the wall up to $y_d^+ = 10$. DR of more than 20% is achieved for $10 \leq y_d^+ \leq 17$. Even at $y_d^+ = 20$, the effectiveness of opposition control does not deteriorate much. However, there is a sudden decrease in DR when the detection plane moves just a little further away from the wall; at $y_d^+ = 23$, the opposition control becomes unstable and a substantial drag increase is observed. The sudden deterioration of the opposition control is rather surprising because these two detection planes ($y_d^+ = 20$ and 23) are located very close to each other. This can restrict the applicability of the opposition control severely, and is further investigated in the next section.

3.2 Input parameters of opposition control

It is very interesting to examine why the two detection planes at $y_d^+ = 20$ and 23 give such contrasting results from each other. In the opposition control, the wall-normal velocity at a detection plane is used as a control input. The detection plane location determines two important control input parameters: the amplitude and the phase of wall blowing and suction velocity. When a different detection plane location is chosen, both parameters of the control input are changed subsequently. It is worthwhile to note that the amplitude of wall blowing and suction was not considered separately in the previous studies, but only the effect of the detection plane location was studied instead [6, 19, 23].

First, the phase information of the detection plane is considered. Figure 4 shows two-point correlation coefficients, R_{vv}, of the wall normal velocity for several monitoring points (y_d). As expected, for no-control case, the correlation coefficients are generally high when the distance between the two points ($y - y_d$) is small. For example, for $y_d^+ = 15$, R_{vv} values are higher than 0.9 in $10 \leq y^+ \leq 20$, implying a similar amount of drag reduction in $10 \leq y_d^+ \leq 20$. R_{vv} decreases slowly as the distance increases. The correlation between the optimal detection plane location and $y^+ = 25$, where drag increases by 50%, is still as high as 0.7. This shows that two velocity signals with a good correlation can result in

a very different drag reduction. The R_{vv} value between the two detection plane locations at $y_d^+ = 20$ and 23 is 0.96. Considering that drag increases by 17% at $y_d^+ = 23$, while a detection plane at $y_d^+ = 20$ results in a 16% drag reduction, the above correlation value of $R_{vv} = 0.96$ is very high. This strongly suggests that the phase information of the detection plane alone cannot explain the sudden change in drag reduction observed between $y_d^+ = 20$ and 23. The effect of blowing and suction amplitude is examined in the next section.

3.3 Amplitude of wall blowing and suction

It is well known that the wall limiting behaviour of the v velocity component is proportional to y^{+2} [29]. As a result of this, the wall-normal velocities at different detection plane locations have different amplitudes. For example, the v' value of a detection plane at $y_d^+ = 23$ is much larger than the value at $y_d^+ = 20$ (see Table 1) while there is little difference in their phase information (see the correlation coefficient graph in Figure 4). Now, the effect of the amplitude of the opposition control on skin friction reduction is investigated for each detection plane location. The detection plane locations are shown in Table 1. Ten different amplitudes ($0.1 \leq A \leq 1$) were chosen for this study. In total, 90 simulations were performed for various amplitudes and detection plane locations, and the results for all cases including the no-control case are shown in Figure 5. This figure clearly demonstrates that the drag reduction in opposition control is affected by the amplitude parameter (A) as well as the detection plane location. With the exception of Iwamoto *et al.* [18] and Chung and Sung [24], only $A = 1$ cases were considered in most previous opposition control studies [6, 19, 23], which corresponds to a vertical line in the figure. It is interesting to see that $A = 1$ cases do not always produce the best drag reduction. In fact, for $y_d > y_{d,op}$ a better drag reduction is obtained at smaller A values and drag reduction deteriorates at larger values of the amplitude parameter. The A value for the largest DR for each detection plane location is shown as a dashed line in the figure. For detection plane locations lower than the optimal value ($y_d \leq y_{d,op}$), the maximum DR is obtained with $A = 1$. It is worthwhile to note that for all detection plane locations considered, an amplitude of $A > 1$ makes the opposition control strategy

unstable and results in a dramatic drag increase.

The results for several y_d^+ values are shown again in Figure 6. With the detection plane at the optimal location ($y_{d,op}^+$), DR increases with the amplitude parameter, having a maximum at $A = 1$. A similar trend is found when the detection plane is located closer to the wall ($y_d < y_{d,op}$); $A = 1$ results in the largest DR for each y_d^+ case. For large A values ($0.5 \leq A \leq 1$), DR does not change significantly, consistent with the previous study [24], which reported that the drag reduction was not affected much when the amplitude was halved. When the detection plane is located further away from the optimal location ($y_d > y_{d,op}$), however, the opposition control is found to be most effective at a small amplitude. With $A = 0.3$, a substantial drag reduction is obtained for $y_d^+ = 25$ and 30. Beyond this A value, the effectiveness of the opposition control deteriorates rapidly, and results in a substantial drag increase. Figure 6 clearly shows that the amplitude plays an important role in the effectiveness of the opposition control.

The use of small amplitude has significant implications for the efficiency of the opposition control. The efficiency of the opposition control can be defined as the ratio of the power saved to the power input [6, 18–20, 30]. Two definitions of the power input to the control are considered. The ideal power input [6] is given as:

$$P_I = \overline{p_w v_w} + \frac{1}{2}\rho \overline{v_w^3}, \tag{4}$$

and a more conservative power input is calculated following Bewley *et al.* [30]:

$$P_{|I|} = \overline{|p_w v_w|} + \frac{1}{2}\rho \overline{|v_w| v_w^2}. \tag{5}$$

The power saved is given as $P_S = (\overline{dP/dx}|_0 - \overline{dP/dx})U_m$. Figure 7 shows the power saving ratio, P_S/P_I and $P_S/P_{|I|}$. A similar level of efficiency was observed as in the previous studies [6, 18, 19] for $A = 1$. With small amplitudes, more power savings and hence better efficiency are obtained for $y_d^+ = 15$. The improvement is greater for $y_d^+ = 25$, suggesting that the amplitude can play an important role in designing efficient control strategies. Since the power input P_I for the opposition control is proportional to the cube of the wall blowing and suction velocity, the control can be designed to operate at lower

amplitude, where the opposition control is more efficient.

3.4 Controlled flow fields

Controlled flow fields are examined to investigate the effect of wall blowing and suction amplitude on the drag reduction. Two detection plane locations ($y_d^+ = 15$ and 25) are chosen for further analysis. Figure 8 presents velocity and vorticity fluctuation profiles for the optimal detection plane location in global units. The friction velocity for the no-control case, u_{τ_0}, is used to calculate $y_0^+ = y\nu/u_{\tau_0}$. The figure shows that all three components of velocity fluctuation gradually decrease as the amplitude parameter A increases (w' not shown here). It is found that with non-zero amplitudes, the opposition control establishes a virtual wall (defined as a local minimum of v') between the physical wall and the detection plane (see Figure 8b). The virtual wall moves away from the physical wall as A increases. With $A = 1$, the virtual wall is located halfway between the wall and the detection plane [6, 23]. Due to the virtual wall in successful opposition control cases, the v' profiles are moved outward. For $A \geq 0.4$, a plateau appears in the u' profiles just below the virtual wall location, and it becomes more prominent as A increases.

In Figures 8c) and 8d), the amplitude of the opposition control is also found to be related to modification of the streamwise vortices (ω_x' and ω_y'). All three components of vorticity fluctuation decrease as A increases (ω_z' not shown here). For example, the local maximum of ω_x' for $y_d^+ = 15$ is reduced by 25%. The distance between the maximum and minimum $\omega_x'^+$ locations can be interpreted as the average radius of streamwise vortices [5, 31]. For no control turbulent channel flow ($A = 0$), the location for the local minimum ω_x' is at $y_0^+ = 5$ [31]. The local minimum location for ω_x' moves away from the wall as the amplitude parameter increases, suggesting a thickening of the viscous sublayer. For $A = 1$, the minimum ω_x' location is at $y_0^+ = 7.2$, the mid way between the detection plane and the wall. The local minimum and maximum ω_x' values also decrease substantially, indicating the reduced strength of the streamwise vortices [5]. It is interesting that a plateau appeares in the ω_y' component as well (Figure 8d), showing that the weakening

of the streamwise vortices is important in successful opposition control.

When the detection plane is located further away from the optimal location, the response of the flow field to the opposition control is different. Figure 9 shows the velocity and vorticity fluctuations for $y_d^+ = 25$ in global units. It is found that small amplitudes ($A \leq 0.4$) are still effective in reducing the velocity and vorticity fluctuations near the wall. A plateau appears in u' and ω_y' at smaller amplitude, but is less prominent compared to the optimal control case. However, large amplitudes increase the velocity and vorticity fluctuation significantly, resulting in a substantial drag increase. For $A = 1$, $\omega'_{x,max}$ is almost twice the no-control value. No plateau is observed at large amplitudes, implying that the underlying mechanism associated with the opposition control is no longer working. It is interesting to note that v'_{max} decreases for positive drag reduction and increases for negative cases. A virtual wall is formed at all amplitudes (Figure 9b), but the v' values at the virtual wall location are not small, indicating that the virtual wall is less effective in preventing a downwash of high-momentum fluids towards the wall during the sweep events [23]. It is found that the virtual wall moved away from the physical wall as A increased. This trend is similar to the one observed for $y_d^+ = 15$ in Figure 8.

Figure 10 presents velocity and vorticity fluctuation (ω_x' and v') profiles for $y_d^+ = 15$ and 25 in local wall units. All quantities are presented in local wall units: $y^+ = y\nu/u_\tau$, $u'^+ = u'/u_\tau$, and $\omega_x'^+ = \omega_x'\nu/u_\tau^2$. When local wall units are used, the velocity and vorticity fluctuation profiles collapse onto a single curve for $y^+ > 20$; especially, the agreement in u'^+ and $\omega_y'^+$ is remarkable (not shown here). This indicates that the effect of the opposition control is confined to the near-wall region below the centre of streamwise vortices, while the flow field in the core region remains similar to the no-control case, albeit with considerably weakened turbulent structures.

It is found that the location for the local minimum of $\omega_x'^+$ moves away from the wall as A increases, while the location for the local maximum moves in the opposite direction. The minimum $\omega_x'^+$ values are much smaller than the no-control case, while the maximum $\omega_x'^+$ values are not affected by the control, suggesting that the streamwise vortices have a similar strength as the no-control case in wall units but are significantly smaller in size

with reduced turbulence activities near the wall. It is interesting that the velocity and vorticity fluctuations for $y_d^+ = 25$ again collapse onto a single curve at $y_d^+ > 40$, indicating that the effect of the opposition control is still confined to the near wall turbulence. The collapse of v'^+ profiles (Figure 10d) is clearly seen for $y_d^+ > 20$ while the large variation is observed in the near-wall region. This is in clear contrast to the v' profiles in Figure 8b), where the v' profiles show a large increase across the whole domain, and v'_{max} decreases for positive DR and increases for negative DR cases.

Velocity (v, w) vector plots in the y-z plane are shown in Figure 11 to demonstrate the efficacy of the virtual wall. Bright (yellow) colour indicates the positive streamwise velocity fluctuation, and dark (blue) colour negative fluctuation. It is clearly seen that the downwash motion is significantly reduced in the optimal control case (Figure 11b) compared to the no-control case (Figure 11a). For $y_d^+ = 25$ (Figure 11d), the opposition control has failed to create a virtual wall to shied the near-wall region. Instead, the downwash motions are intensified by the action of wall blowing and suction, resulting in high skin-friction. With a small amplitude ($A = 0.3$), the virtual wall becomes again effective in preventing the sweep motion, and the near-wall turbulence activities are weakened significantly (Figure 11c).

Turbulent structures are also clearly affected in the opposition control. λ_2 plots [32] are displayed in Figure 12. Near-wall turbulent structures are weakened in the successful case, while they are strengthened significantly in the $y_d^+ = 25$ and $A = 1$ case. This clearly shows that $A = 0.3$ with $y_d^+ = 25$ is as effective as the optimal control case.

3.5 Relationship between DR and other properties

In this section, the characteristics of the controlled flow are examined to establish the relationship between various flow properties and the amount of drag reduction. Understanding such a link is important in the design of control devices, and could be exploited in the development a future optimal control strategy.

It is already shown in Figure 6 that the amplitude parameter (A) plays an important role in drag reduction. However, the relationship between A and DR depends on the

detection plane location and cannot be described as a single curve. This is partly because a different detection plane location has a different strength of wall blowing and suction (see Table 1). To find a better relationship with DR, rms of wall blowing and suction velocity, v'_w, is examined. Although v'_w increases with A for a given detection plane location, there is one big difference between A and v'_w. The range of v'_w varies considerably for different detection plane locations, while A always changes between 0 and 1. So, the same A value results in different levels of v'_w at different y_d because v'_w increases with y_d. For example, v'_w for $A = 1$ is much larger at $y_d^+ = 25$ than at $y_d^+ = 15$ (see Figure 8). Figure 13 shows the variation of v'_w and DR for various control cases. For $y_d \leq y_{d,op}$, the amount of drag reduction increases monotonically with increasing v'_w. It is found that there is a strong correlation between v'_w and DR when the flow control is effective; the correlation follows closely DR $\sim 1.5v'^+_w$ for $v'^+_w < 0.15$, clearly indicating that the wall blowing and suction strength as well as the detection plane location is important in the opposition control. When v'^+_w increases further ($0.15 < v'^+_w \leq 0.25$), the opposition control becomes less efficient and much stronger blowing and suction are needed for a higher DR. For the $y_{d,op}$ case, DR increases linearly up to 20%, beyond which DR increases only modestly with v'^+_w, and the maximum DR is achieved at $v'^+_w = 0.25$.

When the opposition control is less effective ($y_d > y_{d,op}$), the linear relationship between v'^+_w and DR is still evident, but confined mainly to smaller amplitude. It is interesting that the maximum drag reduction is obtained at around $v'^+_w = 0.25$ for all cases considered. It is worth noting that $v'^+_w = 0.25$ is the wall blowing and suction amplitude of the optimal drag reduction case (*i.e.*, $y_d^+ = y_{d,op}^+$ and $A = 1$). Beyond this amplitude ($v'^+_w > 0.25$), DR decreases with v'^+_w for the all detection plane locations considered. This figure shows that there exists a strong correlation between v'^+_w and DR for successful drag reduction cases ($y_d \leq y_{d,op}$), but the correlation becomes weaker and the data are scattered for less efficient cases ($y_d > y_{d,op}$).

To find a better correlation between the flow properties of the opposition control and DR, various flow properties are examined. Among all properties tested, the maximum values of v' and ω'_y display the strongest correlation with drag reduction. Figure 14a shows the variation of wall normal velocity fluctuations in global units, v'_{max}, for various

drag reduction cases. This clearly shows that v'_{max} is closely related to the skin friction drag. v'_{max} is almost linearly proportional to negative drag reduction. It is interesting that a strong correlation between v'_{max} and DR is found for both positive and negative drag reduction cases (see also Figures 8b and 8d). The spanwise velocity fluctuation, w'_{max}, also displays a similar trend (not shown here), and a slightly weaker correlation is observed between w'_{max} and DR. It is interesting to note that v'^{+}_{max} in wall units does not produce as good a correlation as v'_{max}.

The relationship between the local maximum values of wall normal vorticity fluctuations (ω'_y) and DR is also presented in Figure 14b. This figure clearly shows that there exists a strong relationship between $\omega'_{y,max}$ and DR. When the DR is positive, drag increases with $\omega'_{y,max}$: $-\mathrm{DR} \sim 0.4\omega'_{y,max}$. Drag increases more sharply when DR is negative: $-\mathrm{DR} \sim 0.7\omega'_{y,max}$. This figure shows that the skin friction drag is closely related to the near-wall vortical structures in the turbulent boundary layer. This result supports the recent efforts to manipulate the near-wall streamwise vortices for drag reduction.

4 Conclusion

The separate effects of the amplitude and the detection plane location of opposition control were investigated. Direct numerical simulations were performed with various detection plane locations and wall blowing and suction amplitudes. The amplitude of wall blowing and suction as well as the detection plane location was found to be important in the effectiveness of the opposition control. By changing the amplitude of the wall blowing and suction, a substantial drag reduction was achieved for all detection planes located at $5 \leq y_d^+ \leq 30$. The virtual wall was formed in all control cases, but less effective in weakening a downwash of high-momentum fluids towards the wall when wall blowing and suction amplitude was too large. A good correlation between wall velocity fluctuation, v'^{+}_{w}, and drag reduction was found when the opposition control was effective: $\mathrm{DR} \sim 1.5v'^{+}_{w}$. For all successful control cases, the drag reduction increased linearly with the amplitude of wall blowing and suction for $v'^{+}_{w} < 0.15$, and a maximum drag reduction was achieved at around $v'^{+}_{w} = 0.25$. The results show that there existed a maximum

wall blowing and suction amplitude ($v_w'^+ = 0.25$), beyond which DR decreased for the all detection plane locations considered. The characteristics of the controlled flow were also examined to understand the underlying mechanism for drag reduction. In all cases considered, the drag reduction is found to be inversely proportional to the maximum value of the wall normal velocity fluctuations, v'_{max}. The maximum vorticity fluctuation $\omega'_{y,max}$ also had a strong correlation with DR, reinforcing the view that an efficient control strategy should focus on the weakening of streamwise vortices.

Acknowledgement

This work was supported by the Engineering and Physical Sciences Research Council (EPSRC) through the UK Turbulence Consortium (Grant EP/G069581/1), and by the Department of Health through NHS Physical Environment Research Programme (Grant B(08)06). TT was sponsored by the Pakistani government.

References

[1] H. Bieler, A. Abbas, J.-Y. Chiaramonte, and D. Sawyers. Flow control for aircraft performance enhancements - overview of airbus - university cooperation. AIAA Paper 2006-3692, 2006.

[2] N. Kasagi. Progress in direct numerical simulation of turbulent transport and its control. *International Journal of Heat and Fluid Flow*, 19:125–134, 1998.

[3] M. Gad-el-Hak. *Flow Control: Passive, Active and Reactive Flow Management*. Cambridge University Press, 2000.

[4] S. K. Robinson. Coherent motions in the turbulent boundary layer. *Annual Review of Fluid Mechanics*, 23:601–639, 1991.

[5] A. G. Kravchenko, H. Choi, and P. Moin. On the relation of near-wall streamwise vortices to wall skin friction in turbulent boundary layers. *Physics of Fluids A*, 5(12):3307–3309, 1993.

[6] H. Choi, P. Moin, and J. Kim. Active turbulence control for drag reduction in wall-bounded flows. *Journal of Fluid Mechanics*, 262:75–110, 1994.

[7] D. M. Nosenchuck and G. L. Brown. Discrete spatial control of wall shear-stress in a turbulent boundary-layer. In C. G. Speziale R. M. C. So and B. E. Launder, editors, *Near-Wall Turbulent Flows*, pages 689–707. Elservier, Amsterdam, 1993.

[8] C.-M. Ho and Y. C. Tai. Micro-electro-mechanical-systems (MEMS) and fluid flows. *Annual Review of Fluid Mechanics*, 30:579–612, 1998.

[9] L. Löfdahl and M. Gad-el-Hak. MEMS applications in turbulencd and flow control. *Progress in Aerospace Science*, 35:101–203, 1999.

[10] N. Kasagi, Y. Suzuki, and K. Fukagata. Microelectromechanical systems-based feedback control of turbulence for skin friction reduction. *Annual Review of Fluid Mechanics*, 41:231–251, 2009.

[11] C. Lee, J. Kim, D. Babcock, and R. Goodman. Application of neural networks to turbulence control for drag reduction. *Physics of Fluids*, 9(6):1740–1747, 1997.

[12] C. Lee, J. Kim, and H. Choi. Suboptimal control of turbulent channel flow for drag reduction. *Journal of Fluid Mechanics*, 358:245–258, 1988.

[13] P. Koumoutsakos. Vorticity flux control for a turbulent channel flow. *Physics of Fluids*, 11(2):248–250, 1999.

[14] T. Endo, N. Kasagi, and Y. Suzuki. Feedback control of wall turbulence with wall deformation. *International Journal of Heat and Fluid Flow*, 21(5):568–575, 2000.

[15] S. Kang and H. Choi. Active wall motions for skin-friction drag reduction. *Physics of Fluids*, 12:3301–3304, 2000.

[16] H. A. Carlson and J. L. Lumley. Active control in the turbulent wall layer of a minimal flow unit. *Journal of Fluid Mechanics*, 329:341–371, 1996.

[17] C. Kim, W. P. Jeon, J. Park, and Choi H. Effect of a localized time-periodic wall motion on a turbulent boundary layer flow. *Mathematical and Computer Modelling*, 15(1):265–268, 2003.

[18] K. Iwamoto, Y. Suzuki, and N. Kasagi. Reynolds number effect on wall turbulence: Toward effective feedback control. *International Journal of Heat and Fluid Flow*, 23:678–689, 2002.

[19] Y. Chang, S. S. Collis, and S. Ramakrishnan. Viscous effects in control of near-wall turbulence. *Physics of Fluids*, 14(11):4069–4080, 2002.

[20] M. Pamiès, E. Garnier, A. Merlen, and P. Sagaut. Response of a spatially developing turbulent boundary layer to active control strategies in the framework of opposition control. *Physics of Fluids*, 19(10):108102, 2007.

[21] H. Rebbeck and K.-S. Choi. Opposition control of near-wall turbulence with a piston-type actuator. *Physics of Fluids*, 13(8):2142–2145, 2001.

[22] H. Rebbeck and K.-S. Choi. A wind-tunnel experiment on real-time opposition control of turbulence. *Physics of Fluids*, 18(3):035103, 2006.

[23] E. P. Hammond, T. R. Bewley, and P. Moin. Observed mechanisms for turbulence attenuation and enhancement in opposition-controlled wall-bounded flows. *Physics of Fluids*, 10(9):2421–2423, 1998.

[24] Y. M. Chung and H. J. Sung. Sensitivity study of turbulence control with wall blowing and suction. In *Turbulence and Shear Flow Phenomena -3*, volume 1, pages 167–172, June 2003.

[25] Y. M. Chung. Unsteady turbulent flow with sudden pressure gradient changes. *International Jounal for Numerical Methods in Fluids*, 47:925–930, 2005.

[26] T. Grundy. An analysis of the fractional step method for solving the Navier-Stokes equations. Master's thesis, School of Enginering, University of Warwick, U.K., 2008.

[27] J. W. Jewkes, Y. M. Chung, and P. W. Carpenter. Modification to a turbulent inflow generation method for boundary layer flows. *AIAA Journal*, 49(1):247–250, 2011.

[28] H. Choi and P. Moin. Effects of the computational time step on numerical solutions of turbulent flow. *Journal of Computational Physics*, 113(1):1–4, 1994.

[29] N. N. Mansour, J. Kim, and P. Moin. Reynolds-stress and dissipation-rate budgets in a turbulent channel flow. *Journal of Fluid Mechanics*, 194:15–44, 1988.

[30] T. R. Bewley, P. Moin, and R. Temam. DNS-based predictive control of turbulence: An optimal benchmark for feedback algorithms. *Journal of Fluid Mechanics*, 447:179–225, 2001.

[31] J. Kim, P. Moin, and R. Moser. Turbulence statistics in fully developed channel flow at low Reynolds number. *Journal of Fluid Mechanics*, 177:133–166, 1987.

[32] J. Jeong and F. Hussain. On the identification of a vortex. *Journal of Fluid Mechanics*, 285:69–94, 1995.

Figure Captions

Figure 1 Schematic diagram of opposition control. y_c is the distance between the wall and the centre of a streamwise vortex (SV).

Figure 2 The time history of the friction Reynolds number, Re_τ, for various detection plane locations with $A = 1$.

Figure 3 Drag reduction for various detection plane locations with $A = 1$.

Figure 4 Correlation coefficient $R_{vv}(y : y_d) =< v(x, y, z), v(x, y_d, z) >$.

Figure 5 Drag reduction as a function of A and y_d^+. A dashed line indicates the A value for the maximum DR for each detection plane location.

Figure 6 Drag reduction with various amplitudes, A.

Figure 7 Power savings ratio at different A values for $y_d^+ = 15$ and 25. a) P_S/P_I and b) $P_S/P_{|I|}$. A horizontal line indicates zero efficiency.

Figure 8 Velocity and vorticity fluctuations with various amplitudes at $y_d^+ = 15$. $A = 0$ represents the no-control case. No control u_{τ_0} is used to calculate y_0^+.

Figure 9 Velocity and vorticity fluctuations with various amplitudes at $y_d^+ = 25$. For legend, see Figure 8.

Figure 10 Velocity and vorticity fluctuations with various amplitudes. a) and b) for $y_d^+ = 15$, c) and d) for $y_d^+ = 25$. The local u_τ is used to calculate y^+.

Figure 11 Vector plots of (w, v) in the y-z plane. a) no-control, b) $y_d^+ = 15$ and $A = 1$, c) $y_d^+ = 25$ and $A = 0.3$, and d) $y_d^+ = 25$ and $A = 1$. Bright (yellow) colour indicates the positive streamwise velocity fluctuation, and dark (blue) colour negative fluctuation.

Figure 12 Iso-surfaces of $\lambda_2 = -0.02$. a) no-control, b) $y_d^+ = 15$ and $A = 1$, c) $y_d^+ = 25$ and $A = 0.3$, and d) $y_d^+ = 25$ and $A = 1$.

Figure 13 The relation between the wall blowing and suction amplitude, $v_w'^+$, and DR. Here, $v_w'^+$ is non-dimensionalised by u_{τ_0}.

Figure 14 The variation of maximum v' and ω_y' values for various control cases.

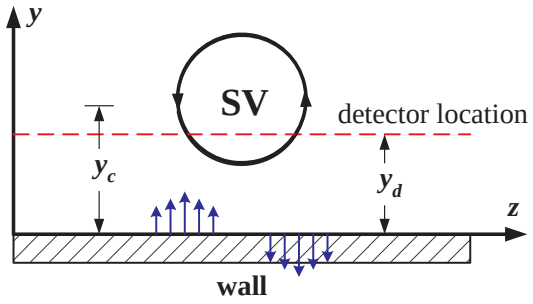

Figure 1: Schematic diagram of opposition control. y_c is the distance between the wall and the centre of a streamwise vortex (SV).

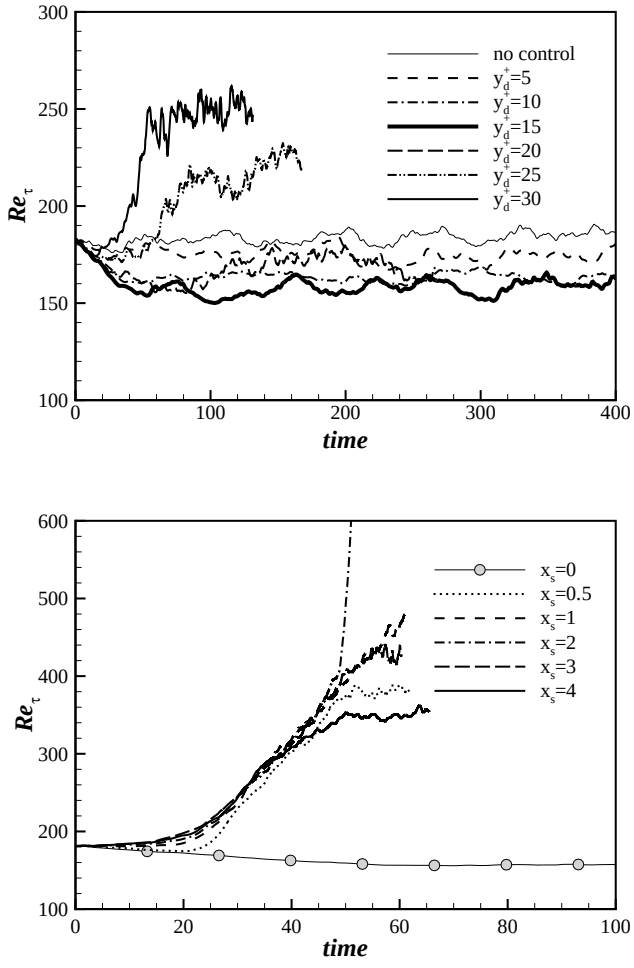

Figure 2: The time history of the friction Reynolds number, Re_τ, for various detection plane locations with $A = 1$.

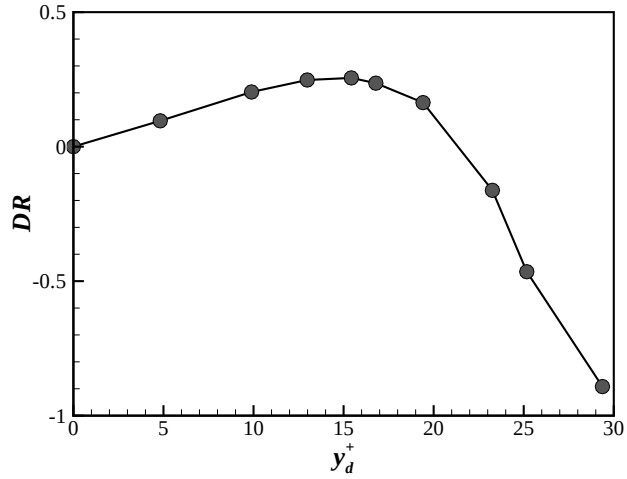

Figure 3: Drag reduction for various detection plane locations with $A = 1$.

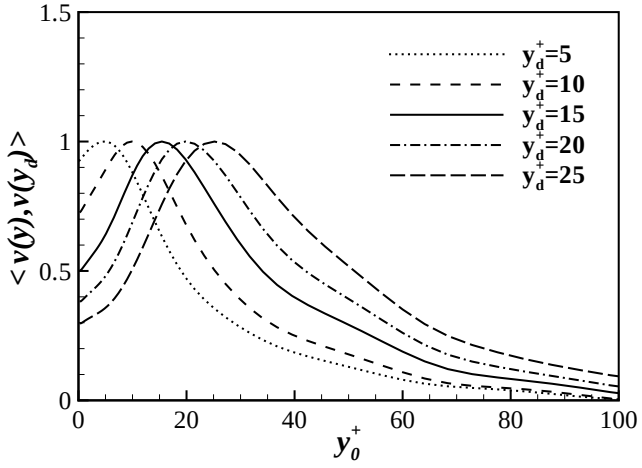

Figure 4: Correlation coefficient $R_{vv}(y : y_d) =< v(x, y, z), v(x, y_d, z) >$.

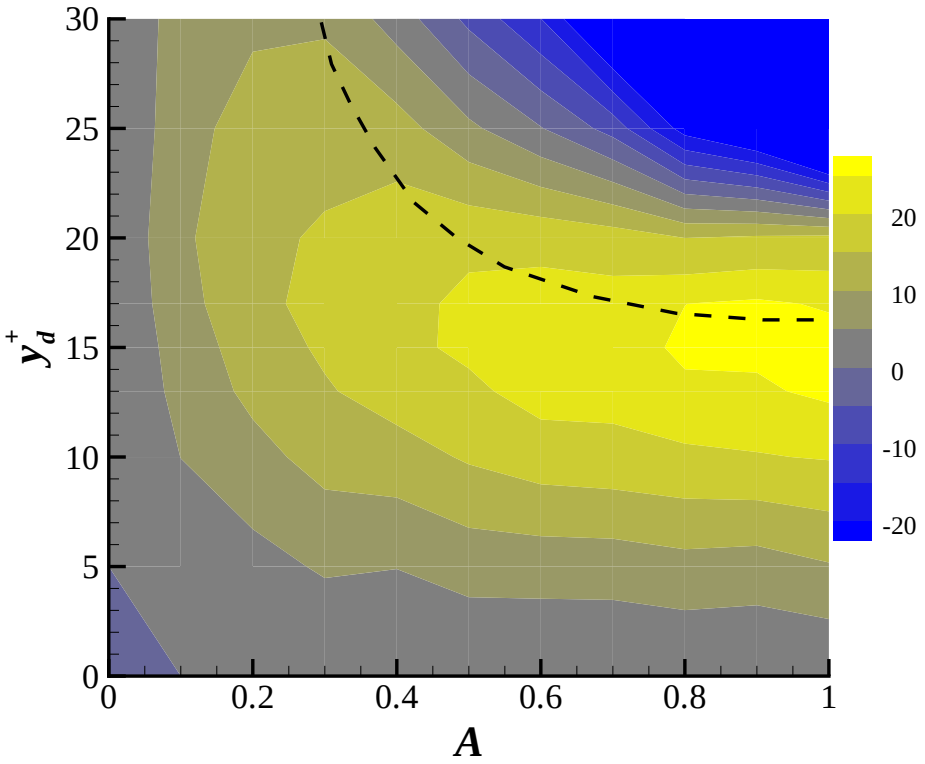

Figure 5: Drag reduction as a function of A and y_d^+. A dashed line indicates the A value for the maximum DR for each detection plane location.

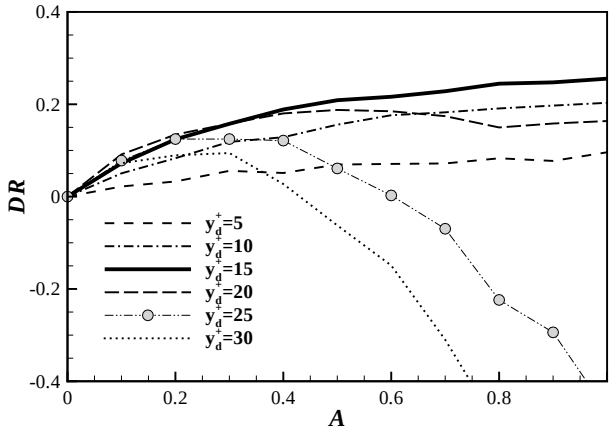

Figure 6: Drag reduction with various amplitudes, A.

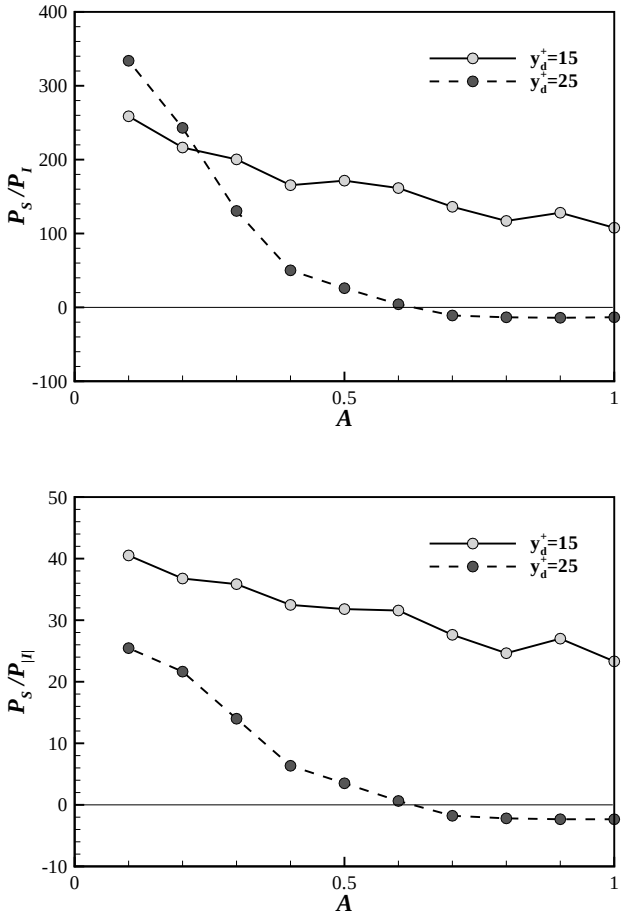

Figure 7: Power savings ratio at different A values for $y_d^+ = 15$ and 25. a) P_S/P_I and b) $P_S/P_{|I|}$. A horizontal line indicates zero efficiency.

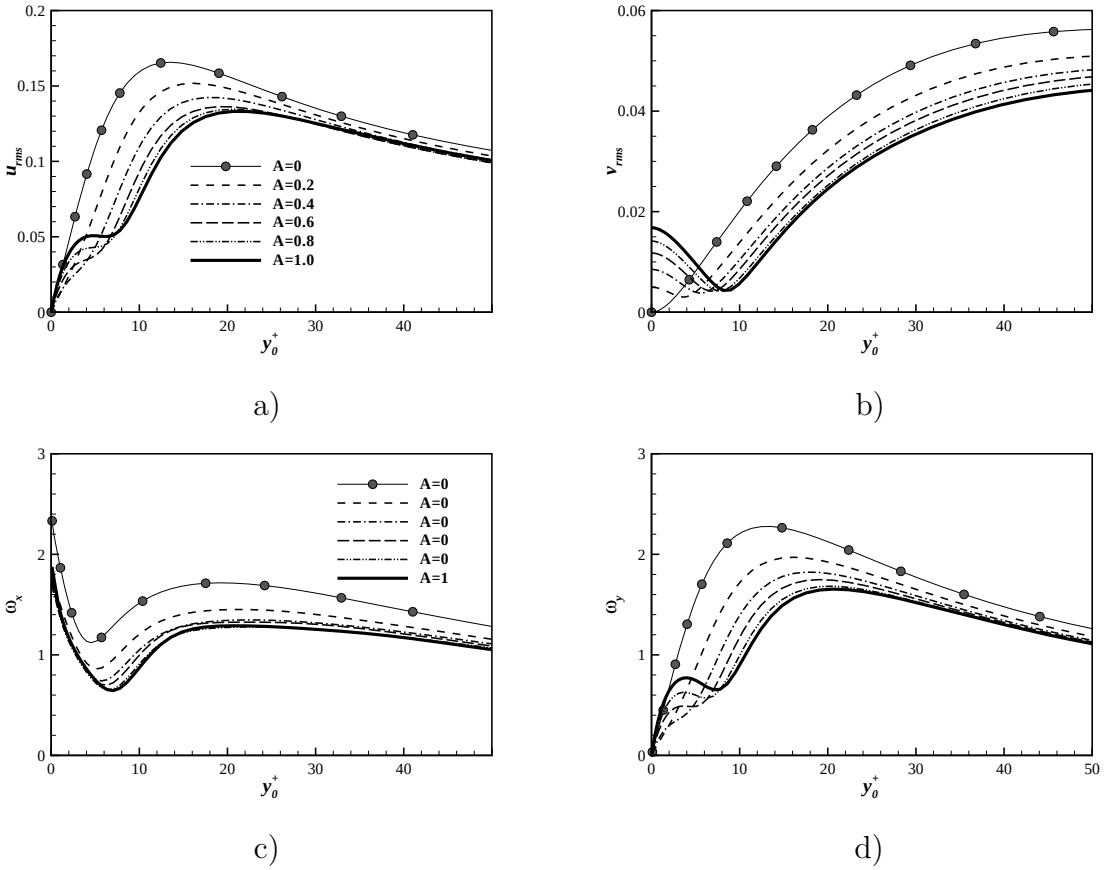

Figure 8: Velocity and vorticity fluctuations with various amplitudes at $y_d^+ = 15$. $A = 0$ represents the no-control case. No control u_{τ_0} is used to calculate y_0^+.

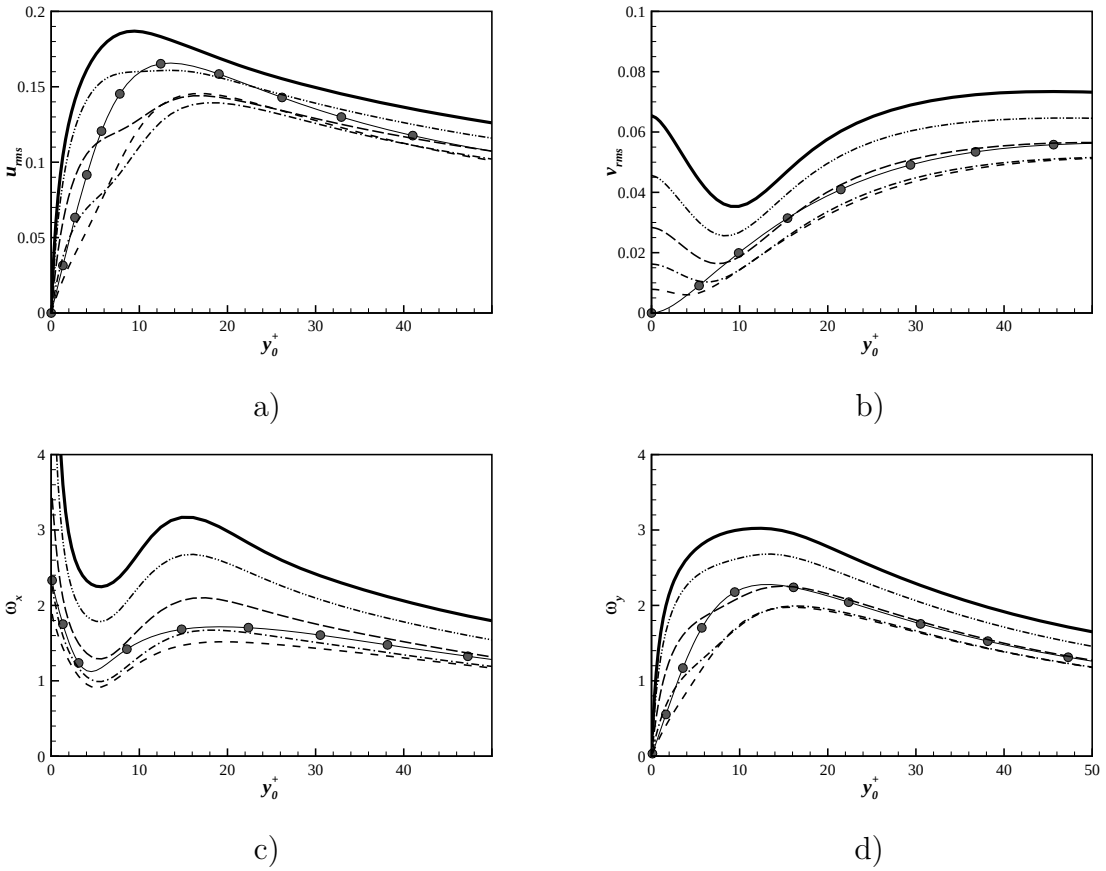

Figure 9: Velocity and vorticity fluctuations with various amplitudes at $y_d^+ = 25$. For legend, see Figure 8.

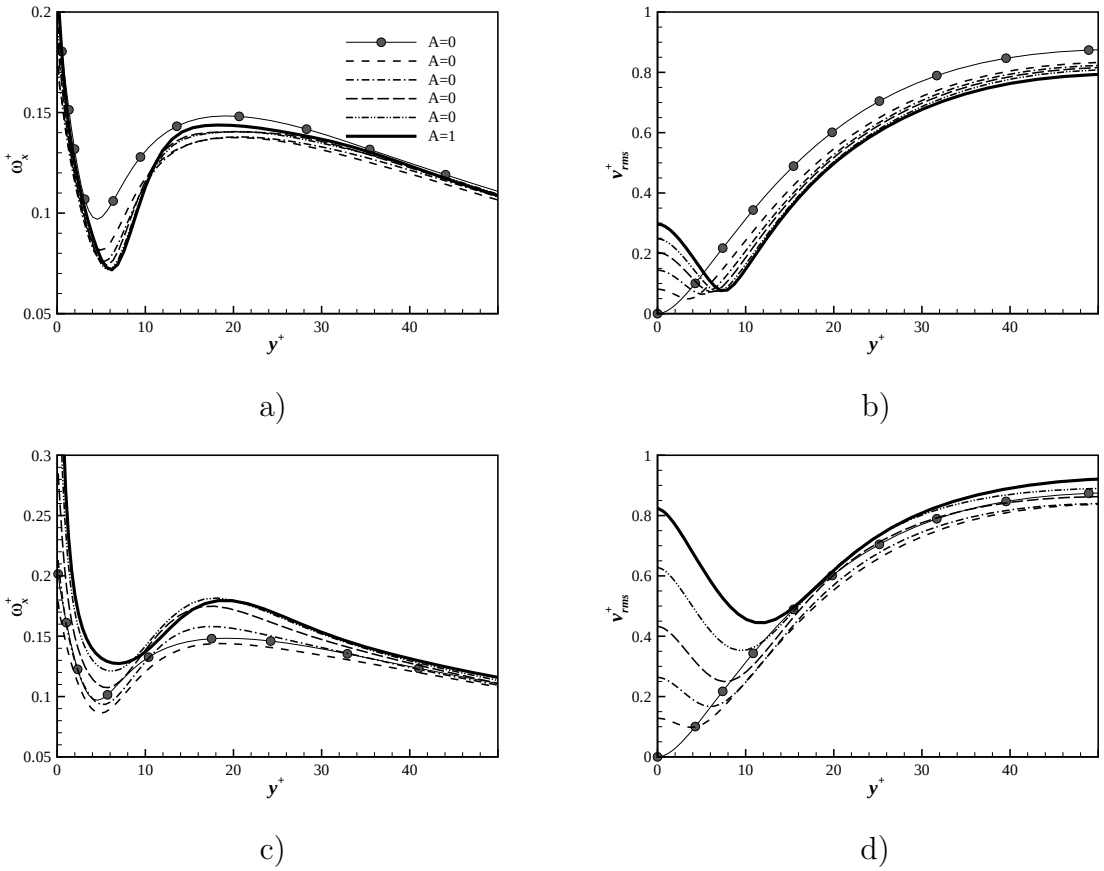

Figure 10: Velocity and vorticity fluctuations with various amplitudes. a) and b) for $y_d^+ = 15$, c) and d) for $y_d^+ = 25$. The local u_τ is used to calculate y^+.

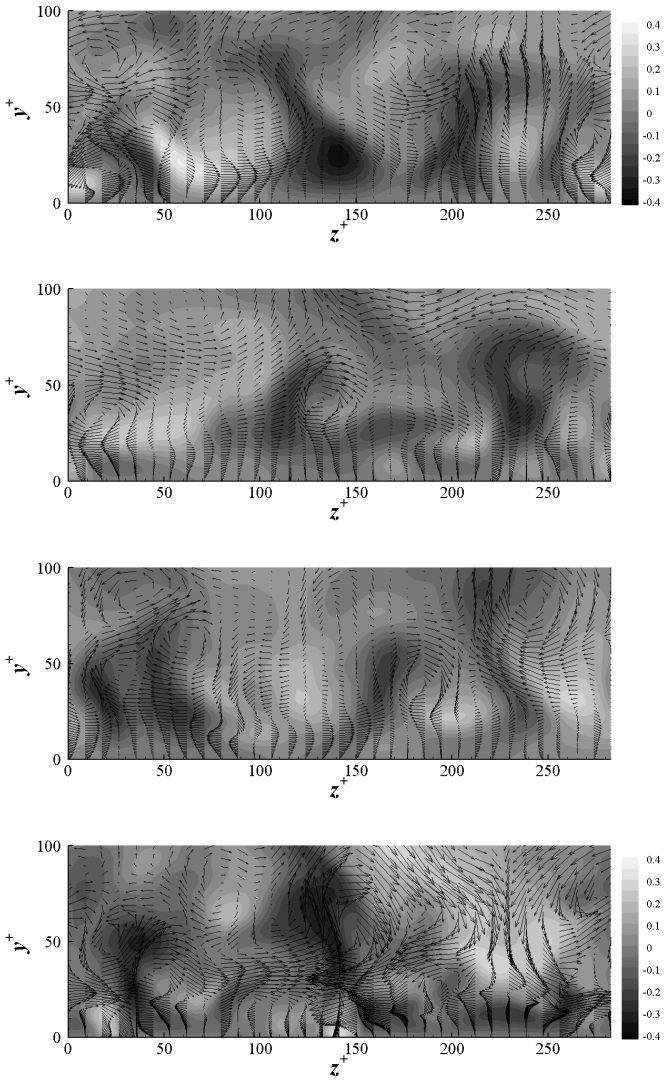

Figure 11: Vector plots of (w, v) in the y-z plane. a) no-control, b) $y_d^+ = 15$ and $A = 1$, c) $y_d^+ = 25$ and $A = 0.3$, and d) $y_d^+ = 25$ and $A = 1$. Bright (yellow) colour indicates the positive streamwise velocity fluctuation, and dark (blue) colour negative fluctuation.

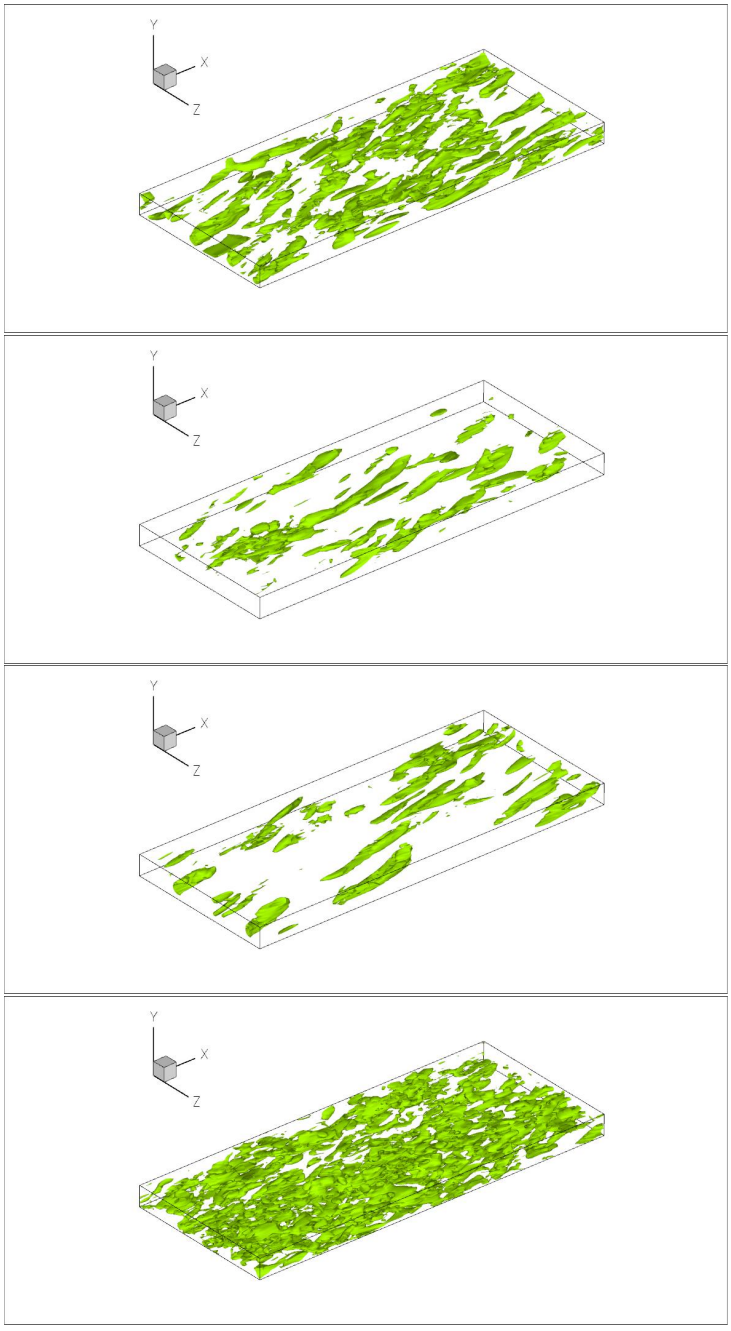

Figure 12: Iso-surfaces of $\lambda_2 = -0.02$. a) no-control, b) $y_d^+ = 15$ and $A = 1$, c) $y_d^+ = 25$ and $A = 0.3$, and d) $y_d^+ = 25$ and $A = 1$.

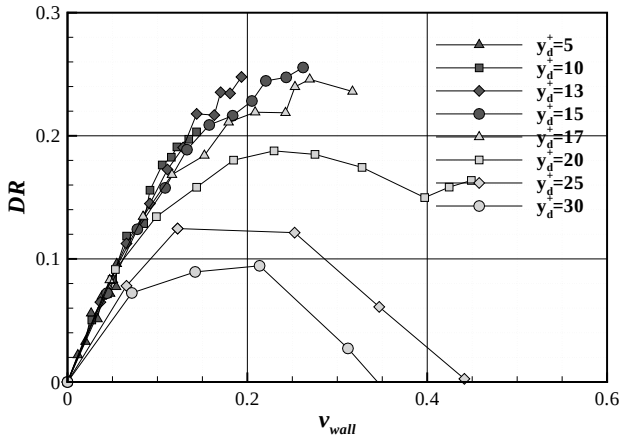

Figure 13: The relation between the wall blowing and suction amplitude, $v_w'^+$, and DR. Here, $v_w'^+$ is non-dimensionalised by u_{τ_0}.

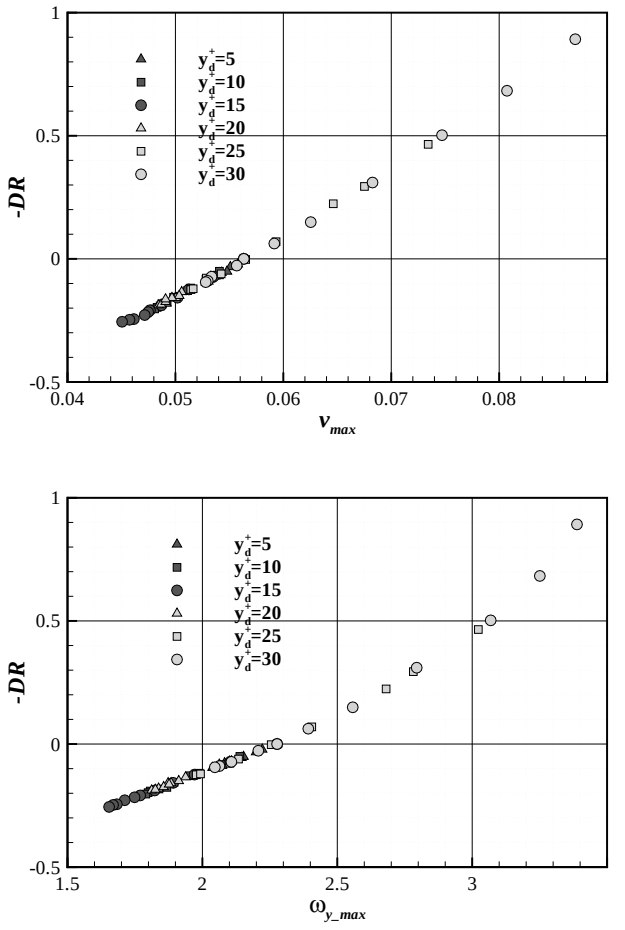

Figure 14: The variation of maximum v' and ω_y' values for various control cases.